



Kaolinite-titanium oxide nanocomposites prepared via sol-gel as heterogeneous photocatalysts for dyes degradation



Lorrana Vietro Barbosa^a, Liziane Marçal^a, Eduardo J. Nassar^a, Paulo S. Calefi^a, Miguel A. Vicente^b, Raquel Trujillano^b, Vicente Rives^b, Antonio Gil^c, Sophia A. Korili^c, Katia J. Ciuffi^a, Emerson H. de Faria^{a,*}

^a Universidade de Franca, Av. Dr. Armando Salles Oliveira, 20, 14404-600-Franca-SP, Brazil

^b GIR-QUESCAT-Departamento de Química Inorgánica, Universidad de Salamanca, 37008-Salamanca, Spain

^c Departamento de Química Aplicada, Universidad Pública de Navarra, 31006-Pamplona, Spain

ARTICLE INFO

Article history:

Received 30 April 2014

Received in revised form 31 July 2014

Accepted 16 September 2014

Available online 4 November 2014

Keywords:

kaolinite
titanium dioxide
photodegradation
methylene blue
methyl orange

ABSTRACT

A purified natural kaolinite was functionalized with titanium(IV) isopropoxide via the hydrolytic sol-gel route and thermally treated at several temperatures, between 100 and 1000 °C, for 24 h. The resulting solids were used for photodegradation ($\lambda=365$ nm, 30 W) of Methylene Blue (MB) and Methyl Orange II (MOII) dyes. All the solids efficiently degraded the dyes and almost total bleaching of the aqueous solutions was observed after 1 h. The best results were found for the solid heated at 400 °C, which degraded 93% of MOII and 99% of MB. Comparative studies with titanium oxide P25 from Degussa were tested and the results reveal lower yields than our systems (45% MB and 15% MOII, 1 h). Kaolinite could promote the dispersion of TiO₂ on the clay surface allowing a fast degradation of dyes. This effect was confirmed by comparison of the results from isolated components (titanium oxide and kaolinite) and titanium oxide-kaolinite nanocomposites.

© 2014 Elsevier B.V. All rights reserved.

1. Introduction

One of the greatest current concerns of humankind is to control and prevent environmental contamination; advanced techniques that can diminish or eliminate pollution, including photodegradation, are mandatory. In this sense, disposal of colored effluents produced by textile, paper pulp, plastic, food and other industries represent a technological problem that affects several countries. It is not easy to estimate the annual amount of waste produced by these industries but some studies indicates that there are over 100,000 types of synthetic dyes available in the market with an output of 7·10⁵ tons per year, and approximately 5–10% is discharged during their production and utilization [1–3].

Azo dyes such as Methyl Orange II (MOII) represent the largest type of textile dyes in industrial use. These reactive azo dyes are not easily amenable by conventional treatment methods due to their stability and non-biodegradable nature. The colored wastewaters released by textile industry effluents pose a potential

environmental hazard to ecosystem and must be treated before being discharged into the natural water bodies [4].

Methylene Blue (MB) is a thiazine cationic dye used for dying silk, leather, plastics, paper and cotton, as well as for the production of ink and copying paper in the office supplies industry. MB has long been used for staining in medicine, bacteriology and microscopy. Although it is not considered to be a very toxic dye, it can cause some harmful effects such as vomiting, increased heart rate, diarrhea, shock, cyanosis, jaundice, quadriplegia, and tissue necrosis on human beings. In this context, MB containing wastewater should be treated by various methods, as the so called Advanced Oxidation Processes [5].

The Advanced Oxidation Processes (AOP) can induce the oxidation of various complex organic compounds such as pesticides, herbicides, drugs and dyes, turning them into products more easily degradable by biological methods. The biological processes associated to AOP can thus become efficient for wastewater treatments. The advantage of these processes is that there is a true destruction of the pollutants and not a transfer of them from one phase to the other, as in other treatments such as adsorption processes. Among the various AOP, heterogeneous photocatalysis involves the use of UV radiation that induces the surface of the semiconductor, such as titanium oxide, zinc oxide, etc., to generate hydroxyl radicals able to oxidize organic compounds considered as contaminants [1–3].

* Corresponding author.

E-mail addresses: mavicente@usal.es (M.A. Vicente), emerson.faria@unifran.edu.br (E.H. de Faria).

The degradation of dyes from effluents is environmentally significant because even small amounts of dyes can sometimes be considered extremely toxic, even if they are not visible. Thus, removal of dyes is not only an environmental challenge, but a public health matter, and the government legislation on water from textile and food industries requires efficient and economically viable processes to remove these pollutants [6–8]. Much confusion exists in the literature about the correct designation of bleaching or mineralization. It is recognized that bleaching is only the simple removal of color from wastewater, not considering the complete oxidation of the organic molecules. Mineralization is considered the complete oxidation of the dye into harmless gaseous CO₂ and of nitrogen and sulfur heteroatoms into inorganic ions, such as nitrate or ammonium, and sulfate ions, respectively [9]. Thus, information about real mineralization of the dye or decreases in toxicity is scarce and therefore much attention has been also focused on the reaction types and mechanisms, based on the identification of the transformation products [10]. The effect of common dye bath constituents on the photocatalytic treatment efficiency has been also discussed in order to examine the application of the photocatalytic degradation on real wastewater effluents.

Heterogeneous photocatalysis with TiO₂ particles is seen as a cutting edge technology, much studied in the last decades in environmental remediation. Some features of this process that make it interesting in wastewater treatment is that it takes place at room temperature, the oxidation is often complete to CO₂, the oxygen required in the reaction is obtained from the atmosphere, the low cost of the photocatalysts and their easy reuse; besides, the process is not selective, which allows to treat complex mixtures of contaminants [1].

There are two major drawbacks for the successful use of the TiO₂-based photocatalysts. First, a high specific surface area is crucial to achieve high activity, as well as a good dispersion of TiO₂ on the matrix surface [2,3]. Some TiO₂-based nanocomposite photocatalysts have shown higher photocatalytic performance than commercial TiO₂ Degussa P25 [11]. It has been remarked that heterogeneous photocatalytic reactions occur on the surface of the catalysts and adsorption of the substrate molecules on the TiO₂ particles is a critical point for their degradation [11–15]. Thus, most studies dealing with photocatalysts based on TiO₂ particles have chosen to disperse them throughout matrices such as silica, alumina, clays or zeolites, in order to increase the number of surface active sites available to generate OH radicals and to improve the interaction with the pollutant [14,15]. Recently, clays are receiving increasing attention as supports of TiO₂-based photocatalysts, as they are able to adsorb organic substances on their external surfaces as well as within their interlamellar spaces [16–24].

In this work, a natural purified São Simão's (Brazil) kaolinite was used to synthesize a new composite with titanium(IV) isopropoxide via the hydrolytic sol-gel route; the materials obtained by thermal treatment at various temperatures were evaluated for the degradation of the two dyes, Methylene Blue (MB) and Methyl Orange II (MOII).

2. Experimental

2.1. Purification of kaolin

The kaolin employed in this work came from the municipality of São Simão, State of São Paulo, Brazil, and was kindly supplied by the mining company Darcy R.O. Silva & Cia. It was purified according to the dispersion-decantation method [25], which yielded very pure kaolinite (see Figure 1), used for further intercalation experiments. In the formulation of the intercalated and grafted compounds, purified kaolinite is abbreviated as *Ka*. All other chemicals were from

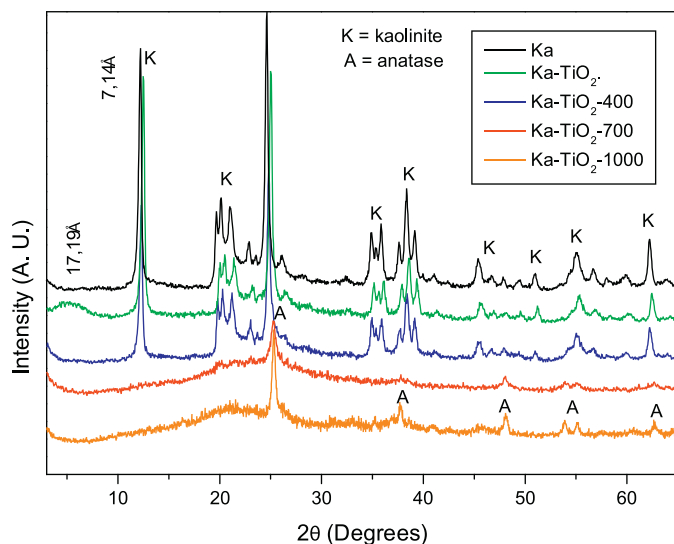


Figure 1. Powder X-ray diffraction patterns of purified kaolinite, and the solids obtained after reaction with Ti(IV) isopropoxide and calcination.

Sigma-Aldrich, Acros Organics and TiO₂ Degussa P25 and were used as received, without further purification.

2.2. Synthesis of photocatalysts

Kaolinite (10.0 g), ethanol (200 cm³), acetic acid (1 cm³), and Ti(IV) isopropoxide (2.0 cm³) were mixed in a beaker, and kept under stirring for 24 h at room temperature. The mixture was washed with distilled water and centrifuged several times, to remove the un-anchored alkoxide from the surface of the clay. The solid was dried at 100 °C for 24 h and split into four fractions, one was used as dried, and the other three were heated in static air at 400, 700, and 1000 °C for 24 h. These temperatures were chosen based on the results from thermal analysis (see Section 3.1.). The sol-gel steps are presented in Figure 2. The expected kaolinite/TiO₂ mass ratio was 1.58, that is very close to the final formula of the nanocomposites, assuming that total hydrolysis and condensation of the alkoxide occurred.

2.3. Characterization techniques

The powder X-ray diffraction (PXRD) diagrams of the solids were acquired in a Siemens D-500 diffractometer operating at 40 kV and 30 mA, using filtered Cu K α radiation and varying 2 θ angle from 2° to 65°. All the analyses were processed at a scan speed of 2° 2 θ /min.

The thermal analyses (TG/DSC) were carried out in a TA Instruments SDT Q600 simultaneous DSC-TGA thermal analyzer, from 25 to 1100 °C, at a heating rate of 10 °C/min and under an air flow of 100 cm³/min.

The Fourier transform infrared absorption spectra were obtained in a Perkin-Elmer Spectrum-One spectrophotometer, using the KBr pellet technique.

Nitrogen adsorption-desorption was carried out at -196 °C using a static volumetric apparatus (Micromeritics ASAP 2020 adsorption analyzer). Prior to the adsorption measurements, the sample (ca. 0.2 g) was outgassed at 120 °C for 24 h under a vacuum better than 0.1 Pa.

Scanning electron microscopy (SEM) was performed using a JEOL microscope (model JSM5610LV). A drop of powder suspension was deposited on a copper grid and the selected area recorded.

The point of zero charge (pH_{ZPC}) was determined by using 5 flasks with 25 mg of each sample, adding aliquots of 1.25, 2.5, 5, 7.5 and 10 cm³ of 0.1 mol/dm³ HCl and other 5 with equal volumes

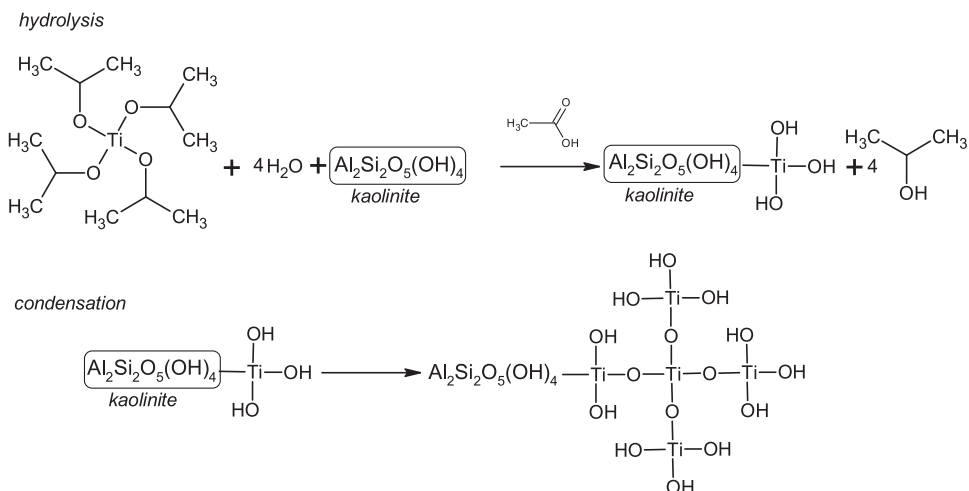


Figure 2. Sol-gel pathways, hydrolysis and condensation reactions, employed in the synthesis of TiO_2 -kaolinite nanocomposite.

of $0.1 \text{ mol}/\text{dm}^3$ NaOH . Subsequently, 5 cm^3 of $0.1 \text{ mol}/\text{dm}^3$ KCl and distilled water up to a volume of 100 cm^3 were added to each flask, including a sample with only KCl $0.1 \text{ mol}/\text{dm}^3$ and water. These samples were shaken for 1 h, after which pH was measured for each sample (pH_1). To each sample, 5 cm^3 of $1 \text{ mol}/\text{dm}^3$ KCl were again added, shaken for 1 h and measured the pH (pH_2). pH_{PZC} value is obtained as the pH to which $\text{pH}_1 = \text{pH}_2$.

2.4. Photodegradation of dyes

The catalysts were dispersed in aqueous solutions of the dyes (50 mg of catalyst in 5 cm^3 of $25 \text{ mg}/\text{dm}^3$ dye solution), and exposed to ultraviolet radiation ($\lambda = 365 \text{ nm}$, $P = 30 \text{ W}$) for 24 h, under constant stirring. The suspensions were then centrifuged, and the supernatants were collected for spectrophotometric analysis. Purified, un-functionalized, kaolinite was also calcined at the same temperature of the catalysts and used for comparative studies. The effect of the experimental parameters time of irradiation, catalyst concentration, dye concentration and pH was analysed to obtain the optimal experimental conditions. The concentration of dyes in the supernatant liquids was determined by ultraviolet-visible (UV-vis) spectroscopy, using a Hewlett-Packard 8453 diode array spectrometer, and the absorption were determined at 486 and 664 nm.

3. Results and discussion

3.1. Catalysts characterization

The powder X-ray diffractograms of the solids are shown in Figure 1. Treatment with Ti(IV) isopropoxide does not produce an increase in the basal distance of kaolinite (7.14 \AA). Direct insertion of the alkoxide into the interlayer region of kaolinite is not expected, due the difficult swelling of this clay because of the hydrogen bonds that maintain the structure of this clay mineral. The remaining diffraction effects, namely, those not depending on the stacking of the layers in the c -dimension, do not change, indicating that the treatment does not alter the structure of each individual layer. The sample treated with Ti isopropoxide and dried at 100°C shows a broad peak at 17.19 \AA , probably related to the deposition of Ti oxy-hydroxide species on the kaolinite surfaces. After calcination at 400°C , this broad peak disappears and the crystallization of TiO_2 begins, while all the characteristic peaks of kaolinite are maintained, giving good evidence that the structure of the clay was maintained. It may be remarked that the characteristic peaks of

anatase are very close to those from kaolinite, which difficult the analysis. After heating at 700°C , kaolinite dehydroxylation occurred and the clay layers collapsed. The phase $\text{Al}_4\text{Ti}_2\text{SiO}_{12}$ was identified; thus, in spite of the chemical inertness of kaolinite, both its octahedral and tetrahedral sheets reacted with the alkoxide to form this mixed phase. After calcination at 1000°C , anatase was formed.

The thermal analysis curves of the dried solid are shown in Figure 3. The thermal analysis results for Ka (not shown) were similar to those reported in the literature, with an initial small endothermic effect at low temperature, 65°C , due to removal of adsorbed water, the elimination of structural water, also endothermic, at 520°C , leading to formation of metakaolinite, and the final transformation to mullite observed at 1000°C [26–32]. The Ka- TiO_2 solid showed a first endothermic effect centered at 66°C , with a mass loss of 4.35%, that is assigned to the removal of adsorbed water and perhaps of small amounts of ethanol, used as a solvent, although the previous drying step should have removed it completely. A second mass loss step, 5.73%, is displayed at 150 – 400°C , and assigned to the decomposition of organic matter, according to the wide exothermic effect observed in the DSC curve close to 400°C . This organic matter should be the acetic acid used in the reaction and/or isopropanol formed by hydrolysis of the alkoxide. Unfortunately we could not analyze the evolved gases, to confirm their specific nature. Condensation between Ti-OH alkoxide groups and Al-OH or Si-OH groups from the clay should also happen in this temperature range, and is probably included in the strong exothermic effect. The process assigned to kaolinite dehydroxylation was centered at 550°C , and the mass loss associated to it decreased from 13.96% in the purified kaolinite to 10.20% in this solid, as expected, due to the lower amount of kaolinite in this solid after addition of the alkoxide. Based on the thermal analysis results, the composition of the composite was estimated to be 19% of TiO_2 and 81% of kaolinite (mass percentages). Papoulis et al. [33] using 70% of titanium in composites synthesized via sol-gel, showed that the kaolinite/ TiO_2 ratio is a crucial factor in determining the degradation efficiency. The mass ratio of the composites synthesized kaolinite/ TiO_2 considering the total hydrolysis and condensation of titanium isopropoxide was 1.30 and is very close to the kaolinite/ TiO_2 ratio planned at the experimental section.

The infrared absorption spectra of the solids are included in Figure 4. The bands at 3653 , 3668 and 3696 cm^{-1} in the spectrum of Ka correspond to interlamellar hydroxyls groups, Al-OH , while the band at 3618 cm^{-1} corresponds to the intralamellar hydroxyl groups. After reaction with titanium isopropoxide, the

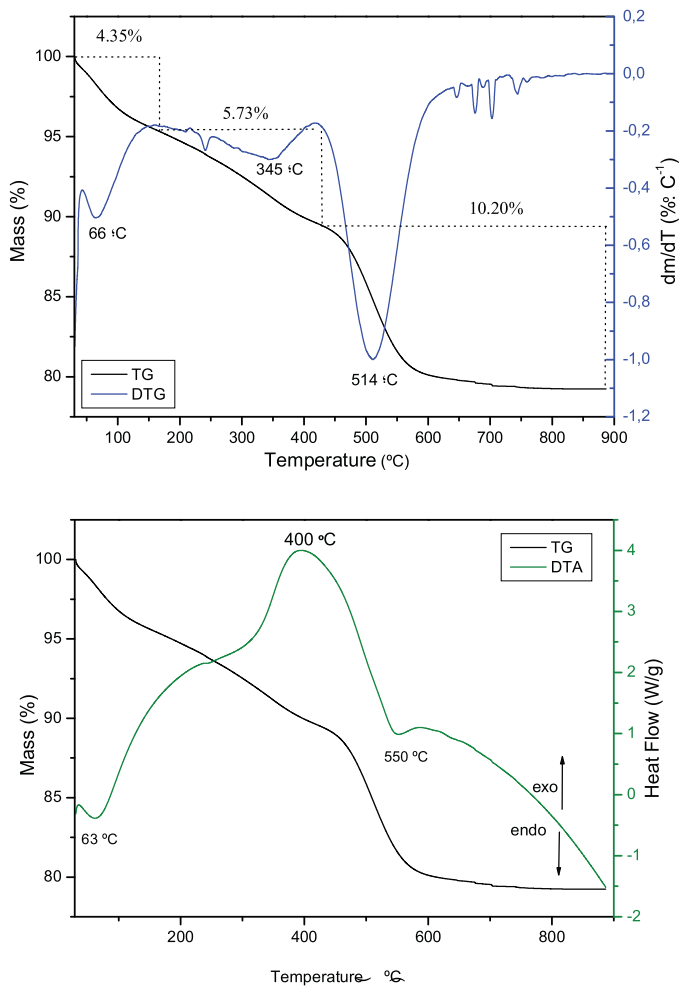


Figure 3. Thermal analyses of Ka-TiO₂ solid.

interlamellar hydroxyl bands were not affected, confirming that the titanium alkoxide interacts with lateral aluminol and silanol hydroxyls. The shift in the positions of hydroxyl vibrations associated to the intercalation or grafting of organic units in the interlayer space of kaolinite layers is well known [26–32]. The characteristic bands of titanium alkoxide and acetate observed at 1200–1900 cm⁻¹ are assigned to symmetric and antisymmetric vibrations of carboxylate groups from acetic acid used as stabilizing agent to the titanium alkoxide. The fact that they were not completely removed by washing suggests that acetate anions should be coordinated to Ti(IV), as carboxylates are good ligands for this cation [34]. Very weak C-H stretching vibrations are also observed close to 2900 cm⁻¹. The spectrum of the solid treated at 400 °C did not show any shift of the hydroxyl bands, while the effects associated to the organic groups were strongly affected. This result is in agreement with the crystallization of a titanium phase observed by PXRD. After calcination at higher temperatures, the bands in the 3200–3700 cm⁻¹ region disappear, evidencing the transformation of kaolinite into metakaolinite, with further development of a broad band at 1050 cm⁻¹ characteristic of SiO₂. Moreover, the change of the band structure in the 1250–400 cm⁻¹ region is the consequence of kaolinite → metakaolinite transformation leading to a change of Al³⁺ coordination from octahedral to tetrahedral [27–32].

The band at 950 cm⁻¹, attributed to the Si-O-Ti antisymmetric stretching vibration, has been proposed as an evidence of the composite formation [15]. This band was not observed in the spectrum of the non calcined solid, probably because Ti⁴⁺ is still coordinated to acetate anions and the Si-O-Ti bonds are not still formed.

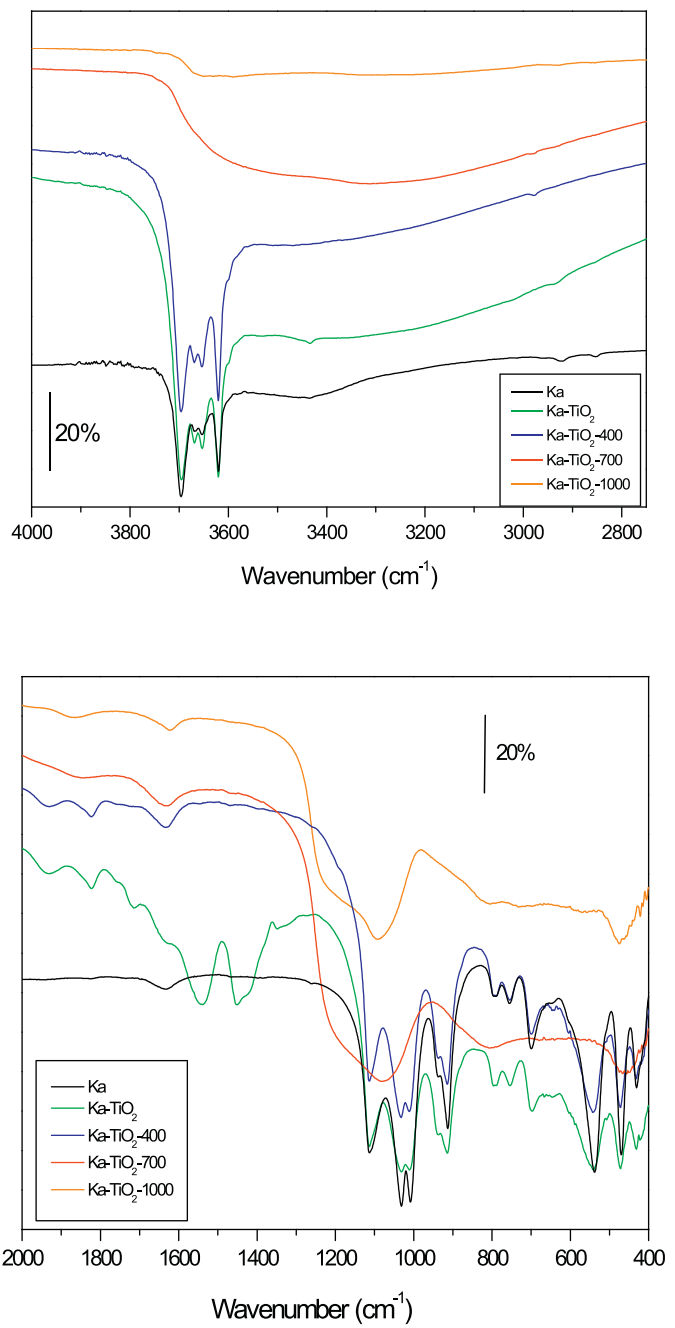


Figure 4. FTIR spectra of the solids in the regions 2750–4000 and 400–2000 cm⁻¹.

However, the band is evident after heating at 400 °C, confirming the formation of the crystalline phase. The bands at ca. 1635 and 3400 cm⁻¹, due to adsorbed water, disappear upon heating. The bands at 1060, 1130 and 1200 cm⁻¹ in the spectrum of the dried solid are very similar to the bending vibration of Ti-O-H in the anatase phase [35,36].

The morphological changes induced by functionalization are clearly observed in Figure 5, in which the SEM micrographs of the composite are shown. Kaolinite particles were typical for this material, showing a flake aspect, grouped forming hexagonal plates and stacks. These hexagonal plates were affected by the functionalization process with the titanium alkoxide; the hexagonal structure was disintegrated in smaller particles, leading to separation of the plates. This fragmentation is increased by the thermal treatment,

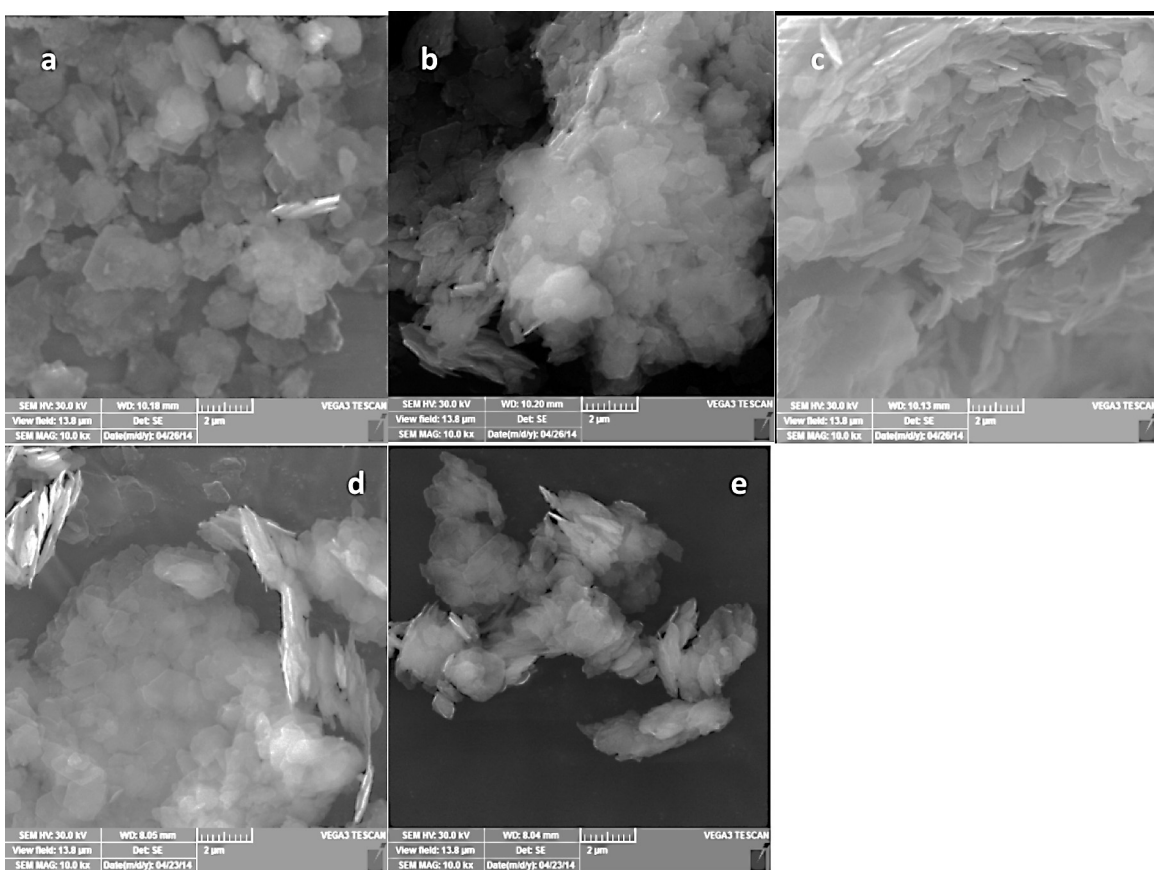


Figure 5. SEM images with magnification of 10.000X of Ka (a), Ka-TiO₂ (b), Ka-TiO₂-400 (c), Ka-TiO₂-700 (d) and Ka-TiO₂-1000 (e).

the faces of the crystals show fissures and agglomeration of the disintegrated smaller particles.

Although several authors aimed to prepare the photocatalytic nanoparticles in the 2:1 phyllosilicates interlayer space [37–39], it is evident that for photocatalytic reactions the most efficient TiO₂ nanoparticles are those which are in direct contact with the pollutant. This requirement is fulfilled by the particles anchored on the edges and the external surface of the particles of the kaolinite matrix.

The nitrogen adsorption–desorption results are shown in Figure 6, while the quantitative data calculated are summarized in Table 1. The isotherms for the purified kaolinite belong to the Type III, with the presence of a hysteresis loop typical of the mesoporous structure of this clay [40]. The presence of titanium alkoxide increases the specific surface area, probably because the titanium alkoxide anchored to the surface of kaolinite creates new positions able to adsorb nitrogen. The BET specific surface area decreases when heating the solids, although the formation of evolution of Ti-phases makes this surface to be relatively high up to 700 °C. The changes in the specific surface area values could be related to the agglomeration of kaolinite platelets, to the textural changes

of kaolinite with the thermal treatment, and also with the formation of an amorphous phase of titanium which can change with the temperature and justify the evolution of the specific surface area.

Titanium alkoxide does not affect the interlayer space of kaolinite but it is well dispersed and located on the external surface of the kaolinite particles. A good distribution of the Ti-containing particles is promissory for the application of this material as a heterogeneous photocatalyst. As proposed by Kocí et al. [11], kaolinite particles can act as an immobilizer preventing the formation of TiO₂ particle aggregates and hence increasing the effective surface area and

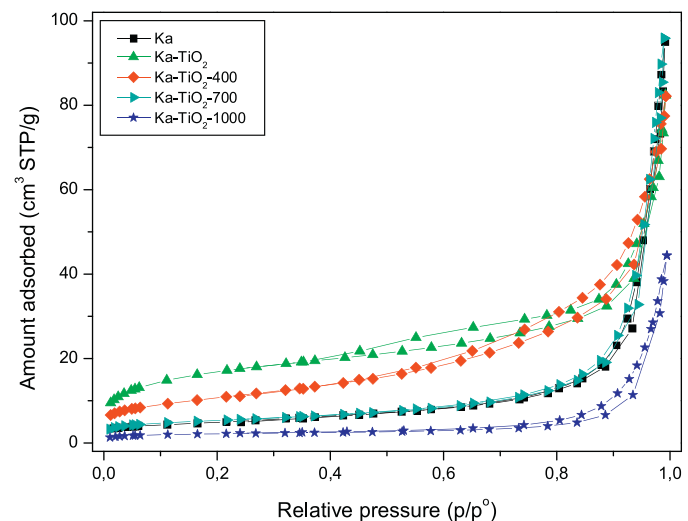
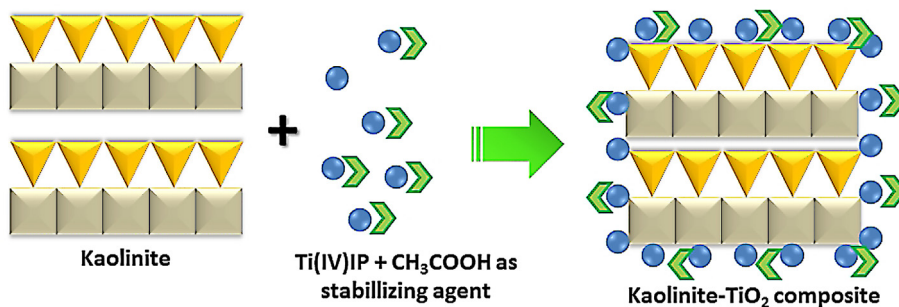
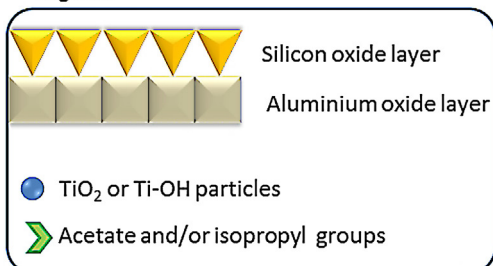


Figure 6. Nitrogen adsorption-desorption data for the catalysts at -196 °C.

Table 1

Specific surface area, average pore size and pore volume of kaolinite and composites with TiO₂.

Sample	Specific surface area (m²/g)	Pore size (Å)	Pore volume (cm³/g)
Ka	17	135	0.127
Ka-TiO ₂	56	91	0.127
Ka-TiO ₂ -400	16	354	0.144
Ka-TiO ₂ -700	26	218	0.140
Ka-TiO ₂ -1000	7	394	0.069

1st step: Synthesis**Legend:****2nd step: Thermal treatment**

Removal of isopropyl radical
and acetic acid
Low amount of particles
agglomeration

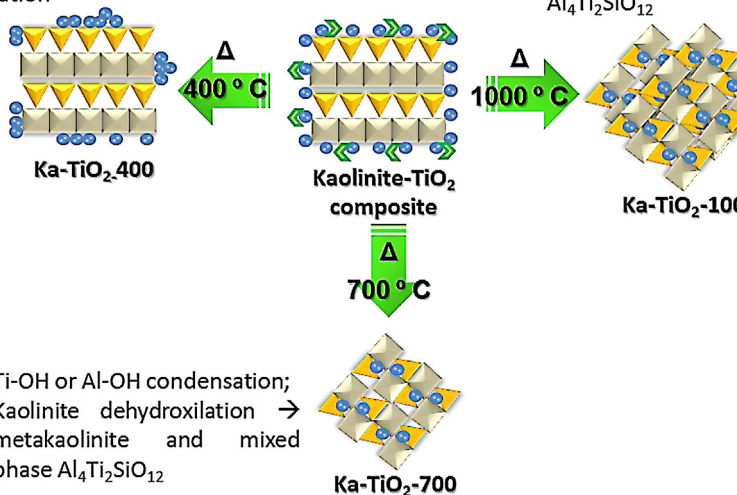


Figure 7. Schematic representation of the preparation of the composites.

photocatalytic efficiency. Catalyst improvement via immobilization might be also due to the force field between the support and the TiO_2 particles that inhibits the recombination of electron-hole pairs [41,37]. The reactions occurring during the synthesis procedure are schematically shown in Figure 7. The detailed reactions of sol-gel transition involved in the preparation of the photocatalysts are shown in Figure 2.

The tendency of the surface to adsorb positively or negatively charged species depends on the concentration of protons in the solution. In this sense, the surface charge characteristics of clay minerals are essential in order to understand the mechanism of adsorption and/or desorption of contaminants such as dyes,

metal ions or pesticides by clay particles, weathering of rocks and deposition of sediments in aqueous medium. The point of zero charge (pH_{PZC}) is the pH value at which the electric charge of the surface becomes null, and is crucial to evaluate the effect of pH on degradation of dyes in the presence of semiconductor oxides that can influence the acid-base equilibrium of the surface chemistry in water systems as shown by the following reactions:

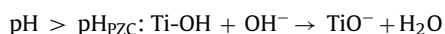


Table 2
Point of zero charge of the kaolinite-TiO₂ catalysts.

Photocatalyst	pH _{ZPC}
Ka	3.1
Ka-TiO ₂	4.1
Ka-TiO ₂ -400	4.4
Ka-TiO ₂ -700	4.3
Ka-TiO ₂ -1000	4.5

where pH_{ZPC} is the zero point of charge of the semiconductor. The point of zero charge of the TiO₂ anatase is reported at about 6.0. The points of zero charge for the materials prepared are summarized in Table 2. The effect of pH on the photocatalytic activity can be explained in terms of the electrostatic interaction between the active photocatalyst sites and the substrate molecules [42]. This interaction can be expected to affect the collision probability of the resulted hydroxyl radical with the molecules. It is stated that the overall reaction would be improved or restrained depending on whether attractive or repulsive forces prevail, respectively. At a pH higher than 4.1, the electrostatic attraction force between dyes and positively charged TiO₂ will improve the maximum photocatalytic activity, and thus lead to a higher degradation efficiency of both dyes. Obviously depending also on the stability, and charge of each dye ($pK_a(MB) = 3.8$ and $pK_a(MOII) = 3.47$). At higher pH, the dye molecules will present negative charges, which led to repulsion of the nanocomposite particles and can promote a decrease in the photocatalytic activity.

3.2. Photocatalytic reaction

3.2.1. Photolysis test and degradation with commercial TiO₂ Degussa P25

For the evaluation of dye degradation exclusively induced by UV radiation, a solution of each dye was submitted to UV radiation in the absence of catalysts, and the degradation performance was evaluated. In both systems, very low degradation ratios, lower than 1%, were observed, evidencing that the presence of the catalysts will play a crucial point in the photodegradation pathway. So, it may be considered in all the reactions that about 1% of the each dye was removed by photolysis. The same test carried out using commercial TiO₂ Degussa P25 as catalyst showed a high efficiency, with about 50% degradation of the dyes after 2 h of reaction, and total degradation after 12 h. This result is similar to that reported by Houas et al. [9], who did not observe direct photolysis for dyes. These authors discussed that photolysis could be neglected with respect to their corresponding photocatalysis.

3.2.2. Reactions conducted without UV-radiation

As mentioned in the experimental section, control reactions were also carried out using the catalysts but without UV-radiation. Low adsorption of the dyes was observed, even after 24 h. The adsorption was much higher for MB than for MOII for all the solids, which is probably related to the anionic character of the second dye, that strongly difficults its interaction with the negatively charged layers of the clay. For MB, the adsorption was significant on the dried solid and, especially, for the solid calcined at 400 °C, with maximum adsorption capacities, q_e , of 44.01 and 45.89 mg/g, respectively. Calcination at higher temperatures decreased the adsorption capacity, to 20.05 and 5.20 mg/g for the solids Ka-TiO₂-700 and Ka-TiO₂-1000, respectively, which is compatible with the effects observed in these solids by X-ray diffraction. As already indicated, the adsorption capacities for MOII were very low, lower than 2 mg/g, for all the solids.

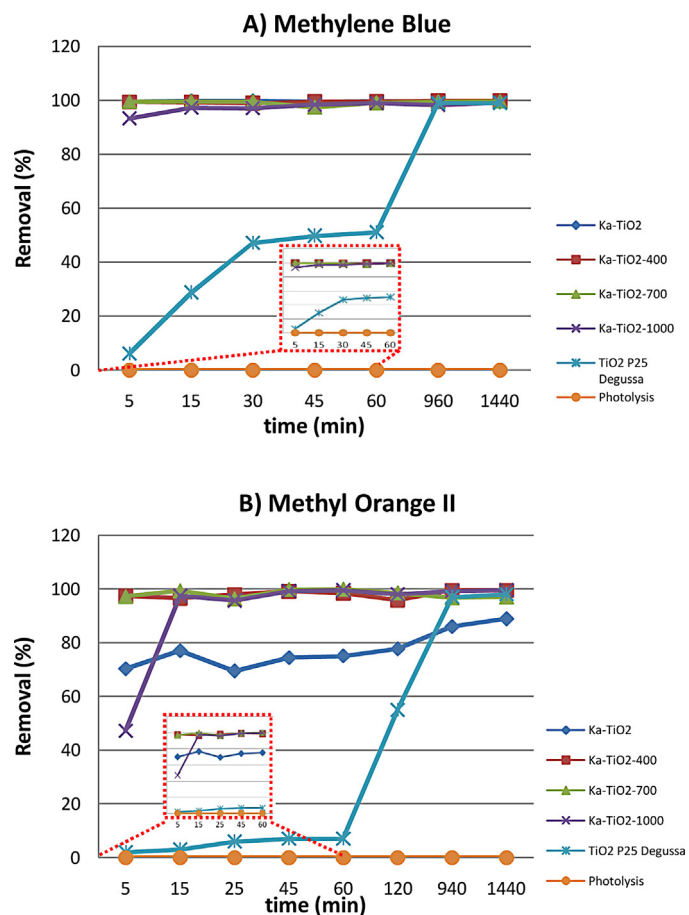


Figure 8. Photocatalytic degradation of MB (A) and MOII (B) by TiO₂-kaolinite composites. Inset: Detail of the removal at 5–60 min. Concentration of the solutions: 25 mg/dm³; mass of catalyst: 50 mg; UV radiation: 365 nm.

3.2.3. Photodegradation of dyes using the kaolinite-titanium oxide nanocomposites

The degradation of the dyes by the kaolinite-TiO₂ composites, compared to the reference experiments above described, is also shown in Figure 8. All the composites showed high degradation performances, even higher than the commercial TiO₂ at short reaction times, although at long reaction times all the catalysts were able to completely degrade the dyes.

Commercial TiO₂ Degussa P25 showed a low photodegradation activity both for MB and MOII, being only 10% after 1 h under UV irradiation, increasing to about 50% after 2 h, and finally reaching 100% degradation after 16.7 h. Degradation of MB was slightly faster than that of MOII.

All titanium based materials here prepared showed a high degradation performance, with a very fast increase of degradation at short time, reaching 100% degradation after only 1 h. Among the several composites, all of them showed a very similar behavior against MB, while against MOII, the dried solid, Ka-TiO₂, showed the lowest activity, which was intermediate between those from commercial TiO₂ and the calcined composites. All the calcined composites showed a very similar behavior. These results are similar to those reported by Chong et al. [41] and Mamulová Kutláková et al. [15]. These authors also prepared kaolinite-TiO₂ composites by the hydrolytic sol-gel method, and obtained higher photo-degradation activity than for TiO₂ Degussa P25.

As previously discussed by Sleiman et al. [43], and confirmed in our previous work using kaolinite with dipicolinate complexes [44], the initial steps of the dye degradation reaction generally involve

the hydroxylation and cleavage of -NH- bonds, resulting in the formation of benzene, aniline and phenol; these byproducts were not evidenced during the kinetic experiment due the fast degradation of the dyes.

As indicated above, the photodegradation activity increased for the solids calcined at 400 °C or higher temperatures. The solid dried at 100 °C showed a lower activity, in spite that it showed the highest adsorption capacity, being colored after centrifugation. The lowest photocatalytic activity of this solid may be related to the fact that titanium ions are not forming a crystalline phase, but is still coordinated to hydroxyl, alkoxide or acetate groups. Thus, calcination at a temperature high enough to form a crystalline phase seems to be a key step to improve the catalytic behavior. Between the two crystalline phases detected, TiO₂ anatase and Al₄Ti₂SiO₁₂, there are not significant performance differences. In addition, the evolution of kaolinite with the calcination temperature should be considered as well: the structure of kaolinite is maintained up to 400 °C, allowing a better dispersion of the photocatalytic sites onto the clay matrix than on metakaolinite at higher temperatures. Metakaolinite formation reduces the specific surface area, generating larger particles of TiO₂. So, considering all these factors, the solid with the best degrading properties, Ka-TiO₂-400, is composed by TiO₂ in the anatase phase and kaolinite, which seems to be the optimum combination to reach the best catalytic results, although its specific surface area is lower than those of the solids dried and calcined at 700 °C. Thus, although the activity performance seems to be a combination of various factors, the nature of the titanium-containing phase is the key factor, followed by the clay phase, while the influence of the specific surface area is somewhat lower. The anionic nature of the layers is probably responsible for the better activity found for degradation of the cationic dye.

Papoulis et al. [14,33,45] have reported the incorporation of TiO₂ particles onto various clay surfaces, such as kaolinites, halloysites and palygorskite. These catalysts were applied for NO gas phase oxidation, faster reaction rates being observed in comparison to commercial Degussa P25 titania. The catalytic behavior is related to the presence of well-dispersed TiO₂, in the form of anatase, on the surfaces of clay minerals. The TiO₂ dispersion is related to the crystal shape and size of the nanoclays. Zhang et al. [13] assigned the high photocatalytic activity of kaolinite-TiO₂ composites to decompose organic compounds to the increase of the specific surface area and development of a mesoporous structure during formation of the composites. These authors also claimed a probable synergic effect between the adsorption promoted by kaolinite layers and the catalytic ability of TiO₂, which enhances the photocatalytic activity.

Thus, the higher photocatalytic activity of the Ka-TiO₂ composites prepared in the present work in comparison to TiO₂ Degussa P25 may be explained by two factors. Firstly, Ka-TiO₂ composites promote a best interaction with MB due to the cationic characteristic of this dye and, secondly, a synergic effect promoted by the interaction between kaolinite and the TiO₂-anatase particles.

Houas et al. [9] evaluated the photodegradation pathways of MB via GC-MS and proposed that titania-based photocatalytic oxidation in water is not selective, by contrast with the selective mild oxidation in pure organic gaseous or liquid phase of aliphatic or substituted aromatic hydrocarbons. Two oxidative agents can be considered: the photo-produced holes H⁺ (mainly involved in the photo-Kolbe de-carboxylation reaction) and/or the OH- radicals, which are known as strongly active and degrading but non-selective agents.

3.2.4. Effect of photocatalyst concentration

The effect of the catalyst concentration was studied by varying the amounts of composite from 25 to 150 mg, in order to obtain an optimum catalyst concentration for the maximum photodegradation. A volume of 5 cm³ of the dye solutions, with concentrations

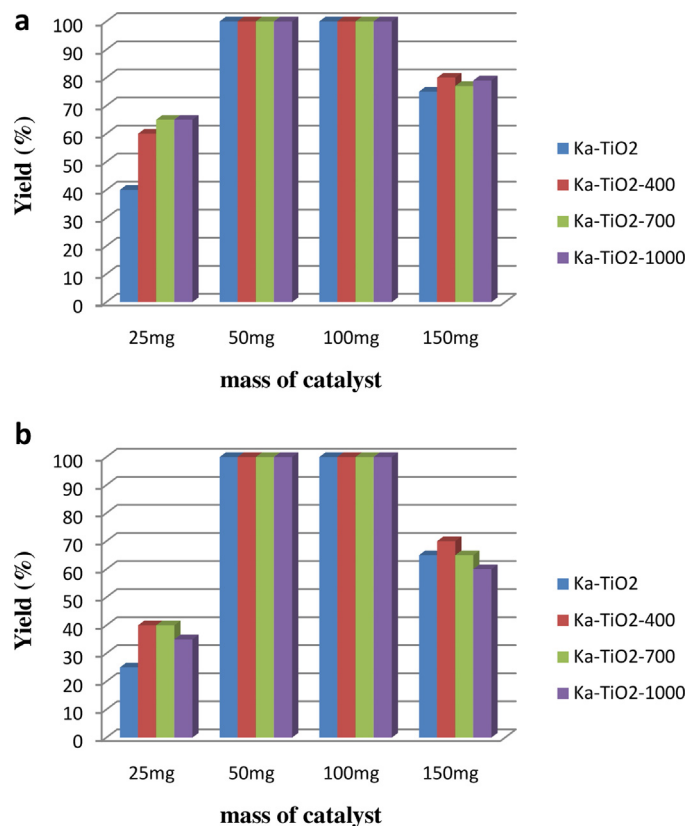


Figure 9. Effect of catalyst concentration for the degradation of dyes MB (a) and MOII (b) using various catalysts based on kaolinite.

of 25 mg/cm³ and a time of 1 h were also selected for these experiments. The results found have been summarized in Figure 9, where it is shown that the degradation efficiency increases up to 100 mg, above which a decrease in degradation efficiency is observed. At a low concentration, the available substrate molecules are not sufficient for the adsorption on the kaolinite-TiO₂ composites. At a high concentration the additional amount of catalyst is not involved in the catalyst behavior and the rate does not increase with an increase in the amount of catalyst [19]. Also, at higher kaolinite-TiO₂ composites amounts, particles aggregation reduces the interfacial area between the reaction solution and the photocatalyst. Thus, the number of active sites on the catalyst surface decreases. The addition of catalyst makes the solution more turbid and promotes the reduction in the degradation efficiency probably due to the reduction in the penetration of light. Other factors as the reactor geometry and the situation of the UV lamp could be not important in the results found. In the present work, 50 mg of catalyst in 5 cm³ of dye solution was found to lead the maximum degradation of dyes.

3.2.5. Effect of the dye concentration

The effect of the initial concentration of the substrate on the degradation of dyes was studied considering values from 10 to 100 mg/cm³. Ka-TiO₂-400 has been selected for this study. Experimental results are presented in Figure 10, which shows that the degradation rate depends on the initial concentration of dyes. The rate of degradation was found to increase with the concentration of dye up to 25 mg/cm³. This behavior could be explained on the basis that, on increasing the concentration of MB or MOII, the reaction rate increases as more molecules of the dye are available for degradation. Also with an increase in dye concentration, the solution becomes more intensely colored and the path length of photons

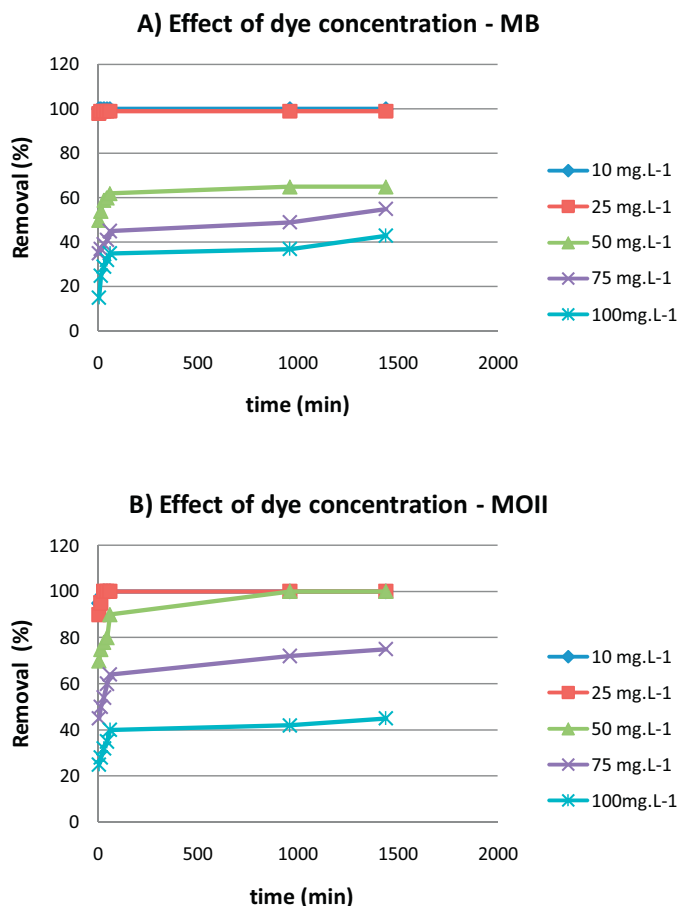


Figure 10. Effect of dyes concentration: MB (a) and MOII (b) in the photodegradation using the catalyst Ka-TiO₂-400.

entering the solution is decreased thereby fewer photons reached the catalyst surface. Hence, the production of hydroxyl and superoxide radicals is decreased [19]. Therefore, the photodegradation efficiency is reduced. At higher concentrations, the number of collisions between dye molecules increases whereas the number of collisions between dye molecules and OH radicals decreases. Consequently, the rate of reaction is retarded. In the present work, the optimal substrate concentration of MB or MOII was found to be between 10 and 25 mg/cm³ when Ka-TiO₂-400 was used as catalyst.

3.2.6. Effect of the pH

pH is a widely studied parameter in the literature. Herein, three pH values have been selected: 3.0, 7.0 and 9.0, and from the results found the amounts of dye adsorbed increased with the pH, while

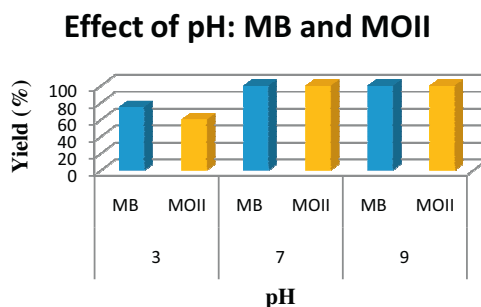


Figure 11. Effect of the pH on the bleaching efficiency of dyes: MB and MOII (25 mg/dm³); volume of solution: 5 cm³; reaction time: 60 min; catalyst: Ka-TiO₂-400 (50 mg).

the disappearance of dye was favoured at basic pH. The pH values are selected taking into account the pH_{PZC} of the materials synthesized and the pKa of the dyes. Using the previously optimized experimental conditions, 50 mg of Ka-TiO₂-400 and 25 mg/dm³ of dye, the effect of the pH on the bleaching efficiency was evaluated. A significant improvement on the bleaching process of MOII at pH between 7 and 9 was observed (see Figure 11). As previously reported by Gouvea et al. in the case of photodegradation of reactive dyes Remazol Brilliant Blue R and Remazol Black B [46], the correct interpretation of pH effects on the efficiency of the photochemical process is very difficult, related to the possible mechanism of reactions that can promote the dye degradation. The three main mechanisms are hydroxyl radical attack, direct oxidation by the positive hole, and direct reduction by the electron in the conducting band. The specific importance of each mechanism depends on the substrate nature, photocatalyst used and pH. In the case of photocatalysts based on kaolinite-TiO₂ nanocomposites, the main reaction may be assigned to the hydroxyl radical attack, which can be promoted by the higher concentration of adsorbed hydroxyl groups at high pH values (> 7). As discussed by Gouvea et al. [46] other explanations can be given for the pH effects and it is probably related to the changes in the speciation of the dye. The deprotonation of the dye can change its adsorption characteristics and redox reactivity.

3.2.7. Evaluation of the influence of the matrix in the photodegradation of dyes

The synergistic effect of the components of the nanocomposite on the bleaching efficiency was evaluated using pure kaolinite,

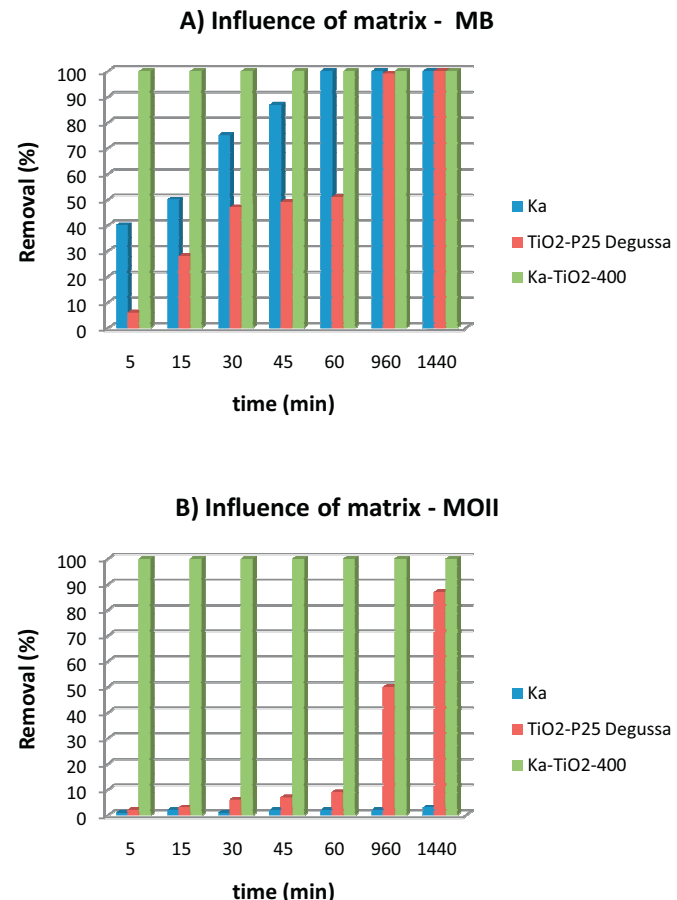


Figure 12. Effect of the matrix on the bleaching efficiency of dyes: MB and MOII (25 mg/dm³); volume of solution: 5 cm³; reaction time: between 5 and 1440 min; catalyst: Ka-TiO₂-400 (50 mg).

TiO₂ Degussa P25 and Ka-TiO₂-400 as photocatalysts in the experimental conditions previously reported (50 mg of catalyst and 25 mg/dm³ of dye). A significant improvement on the bleaching process of MB and MOII was observed for Ka-TiO₂-400 (see Figure 12). In the case of kaolinite with MB, the fast decolorization of the solution was observed, promoted by adsorption. When Ka-TiO₂-400 was used, the solid was completely white, confirming that the initially adsorbed dye can be also degraded by hydroxyl radicals generated on the surface. Kaolinite can act as an immobilizer preventing the formation of TiO₂ particle aggregates and increasing the catalytic efficiency. As expected, a lower adsorption capacity was found for MOII dye, assigned to the anionic characteristics of the molecule and confirming the previous hypothesis described in Section 3.2.2.

4. Conclusions

Kaolinite-TiO₂ composites have been prepared by a sol-gel method, using titanium(IV) isopropoxide as precursor. The thermal treatment of the composite initially formed gave rise to various composites, in which the clay changed from kaolinite to metakaolinite at 700 °C, and titanium was initially forming an amorphous phase, coordinated to hydroxyls, isopropoxide and acetate groups at 100 °C, transforming to anatase at 400 °C, to Al₄Ti₂SiO₁₂ at 700 °C, and again forming anatase at 1000 °C.

This structural evolution strongly affected the catalytic behavior in photodegradation of methylene blue and methyl orange II. The solid calcined at 400 °C, formed by kaolinite and anatase, showed the best behavior. The specific surface area had a minor effect on the catalytic behavior. This activity was higher for the degradation of the cationic dye (MB) than the anionic one (MOII), a fact again related to the nature of the catalysts. All the composites showed higher activities than commercial TiO₂ Degussa P25, especially at short reaction time.

The better photocatalytic activity of the kaolinite-TiO₂ composites is assigned to the presence of well-dispersed TiO₂ (anatase phase), essentially promoted by the low aggregation between the clay matrix and TiO₂ particles, and a synergic effect promoted by the adsorption on the clay matrix, a fundamental step of the degradation mechanism.

Acknowledgments

This work has been carried out in the frame of a Spain-Brazil Interuniversity Cooperation Grant, financed by MEC (PHB2011-0164-PC) and CAPES (267/12), and a Cooperation Grant from Universidad de Salamanca and FAPESP (2013/50216-0). Spanish authors thank additional financial support from Junta de Castilla y León (SA009A11-2) and Ministerio de Economía y Competitividad (MAT2013-47811-C2-R). The Brazilian group thanks support from Brazilian Research funding agencies FAPESP (2011/17660-8 and 2013/19523-3) CAPES and CNPq.

References

- [1] <http://www.psa.es/webeng/index.php>. Plataforma Solar de Almería (PSA). Centro de Investigaciones Energéticas, Medioambientales y Tecnológicas (CIEMAT), Spain.
- [2] B.-Y. Wei, M.-C. Hsu, P.-G. Su, H.-M. Lin, R.-J. Wu, H.-J. Lai, *Sens. Actuators B: Chem.* 101 (2004) 81–89.
- [3] F. Vietmeyer, B. Seger, P.V. Kamat, *Adv. Mater.* 19 (2007) 2935–2940.
- [4] L. Marçal, E.H. de Faria, M. Saltarelli, P.S. Calefi, E.J. Nassar, K.J. Ciuffi, R. Trujillano, M.A. Vicente, S.A. Korili, A. Gil, *Ind. Eng. Chem. Res.* 50 (2010) 239–246.
- [5] R. García-González, A. Costa-García, M.T. Fernández-Abedul, *Sens. Actuators B: Chem.* 202 (2014) 129–136.
- [6] J.D. Wright, N.A.J.M. Sommerdijk, *Sol–Gel Materials Chemistry and Applications*, Taylor & Francis, 2001.
- [7] M. Lucas, P.F.P.T. Jeremias, J. Andreus, I.O. Barcellos, P. Peralta-Zamora, *Quim. Nova* 31 (2008) 1362–1366.
- [8] P. Chowdhury, T. Viraraghavan, *Sci. Total Environ.* 407 (2009) 2474–2492.
- [9] A. Houas, H. Lachheb, M. Ksibi, E. Elaloui, Ch. Guillard, J.-M. Herrmann, *Appl. Catal. B: Environ.* 31 (2001) 145–157.
- [10] I.K. Konstantinou, T.A. Albanis, *Appl. Catal. B: Environ.* 49 (2004) 1–14.
- [11] K. Koci, V. Matejka, P. Kovář, Z. Lacny, L. Obalová, *Catal. Today* 161 (2011) 105–109.
- [12] R. Mathew, S.U. Khan, *J. Agric. Food Chem.* 44 (1996) 3996–4000.
- [13] Y. Zhang, H. Gan, G. Zhang, *Chem. Eng. Journal* 172 (2011) 936–943.
- [14] D. Papoulis, S. Komarneni, D. Panagiotaras, E. Stathatos, K.C. Christoforidis, M. Fernández-García, H. Li, Y. Shu, T. Sato, H. Katsuki, *Appl. Catal. B* 147 (2014) 526–533.
- [15] K. Mamulová Kutláková, J. Tokarský, P. Kovář, S. Vojtěšková, A. Kovářová, B. Smetana, J. Kukutschová, P. Čapková, V. Matějka, J. Hazard. Mater. 188 (2011) 212–220.
- [16] S. Ray, R. Sede, C. Priest, J. Ralston, *Langmuir* 24 (2008) 13007–13012.
- [17] J.C. Zhao, T.X. Wu, K.Q. Wu, K. Oikawa, H. Hidaka, N. Serpone, *Environ. Sci. Technol.* 32 (1998) 2394–2400.
- [18] Q. Wang, C.C. Chen, D. Zhao, W.H. Ma, J.C. Zhao, *Langmuir* 24 (2008) 7338–7345.
- [19] Y.M. Xu, C.H. Langford, *J. Phys. Chem. B* 101 (1997) 3115–3121.
- [20] T.Y. Peng, D. Zhao, K. Dai, W. Shi, K. Hirao, *J. Phys. Chem. B* 109 (2005) 4947–4952.
- [21] S.D. Miao, Z.M. Liu, B.X. Han, J.L. Zhang, X. Yu, J.M. Du, Z.Y. Sun, *J. Mater. Chem.* 16 (2006) 579–584.
- [22] H.L. Hong, W.T. Jiang, X.L. Zhang, L.Y. Tie, Z.H. Li, *Appl. Clay Sci.* 42 (2008) 292–299.
- [23] Z.H. Li, W.T. Jiang, C.J. Chen, H.L. Hong, *Langmuir* 26 (2010) 8289–8294.
- [24] H.M. Yang, A.D. Tang, J. Ouyang, M. Li, S. Mann, *J. Phys. Chem. B* 114 (2010) 2390–2398.
- [25] L.R.D. da Silva, L.C. Garla, *Quim. Nova* 22 (1998) 169–174.
- [26] E.H. de Faria, O.J. Lima, K.J. Ciuffi, E.J. Nassar, M.A. Vicente, R. Trujillano, P.S. Calefi, *J. Coll. Interf. Sci.* 335 (2009) 210–215.
- [27] L.R. Avila, E.H. de Faria, K.J. Ciuffi, E.J. Nassar, P.S. Calefi, M.A. Vicente, R. Trujillano, *J. Coll. Interf. Sci.* 341 (2010) 186–193.
- [28] J. Tunney, C. Detellier, *Clays Clay Miner.* 42 (1994) 473–476.
- [29] J. Tunney, C. Detellier, *Can. J. Chem.* 75 (1997) 1766–1772.
- [30] R.L. Frost, J. Kristof, G. Paroz, J.T. Kloprogge, *J. Phys. Chem. B* 102 (1998) 8519–8532.
- [31] R.L. Frost, J. Kristof, E. Horvat, J.T. Kloprogge, *J. Phys. Chem. A* 103 (1999) 9654–9660.
- [32] S. Letaief, C. Detellier, *Chem. Comm.* 1 (2007) 2613–2615.
- [33] D. Papoulis, S. Komarneni, D. Panagiotaras, E. Stathatos, D. Toli, K.C. Christoforidis, M. Fernandez-Garcia, H. Li, S. Yin, T. Sato, H. Katsuki, *Appl. Catal. B* 132–133 (2013) 416–422.
- [34] N.N. Greenwood, A. Earnshaw, *Chemistry of the Elements*, Second Edition, Butterworth-Heinemann, 1997.
- [35] X. Gao, I.E. Wachs, *Catal. Today* 51 (1999) 233–254.
- [36] T. Bezrodna, G. Puchkovska, V. Shymanovska, J. Baran, H. Ratajczak, *J. Mol. Struct.* 700 (2004) 175–181.
- [37] R. Kun, K. Mogyorosi, I. Dekany, *Appl. Clay Sci.* 32 (2006) 99–110.
- [38] Y. Kameshima, Y. Tamura, A. Nakajima, K. Okada, *Appl. Clay Sci.* 45 (2009) 20–23.
- [39] J. Liu, X. Li, S. Zuo, Y. Yu, *Appl. Clay Sci.* 37 (2007) 275–280.
- [40] N.G. Veerabadran, R.R. Price, Y.M. Lvov, *Nano* 2 (2007) 115–118.
- [41] M.N. Chong, V. Vimones, S. Lei, B. Jin, C. Chow, C. Saint, *Micropor. Mesopor. Mater.* 117 (2009) 233–242.
- [42] M. Gar Alalm, A. Tawfik, *International Journal of Chemical, Nuclear, Metallurgical and Materials Engineering* 8 (2014) 146–149.
- [43] M. Sleiman, D. Vildozo, C. Ferronato, J.-M. Chovelon, *Appl. Catal. B* 77 (2007) 1–11.
- [44] F.R. Araújo, J.G. Baptista, L. Marçal, K.J. Ciuffi, E.J. Nassar, P.S. Calefi, M.A. Vicente, R. Trujillano, V. Rives, A. Gil, S. Korili, E.H. de Faria, *Catal. Today* 227 (2014) 105–115.
- [45] D. Papoulis, S. Komarneni, A. Nikolopoulou, P. Tsolis-Katagas, D. Panagiotaras, H.G. Kacandes, P. Zhang, S. Yin, T. Satog, H. Katsuki, *Appl. Clay Sci.* 50 (2010) 118–124.
- [46] C.A.K. Gouvêa, F. Wypych, S.G. Moraes, N. Durán, N. Nagata, P. Peralta-Zamora, *Chemosphere* 40 (2000) 433–440.